THERMAL-HYDRAULIC ANALYSIS OF LIGHT WATER REACTORS UNDER DIFFERENT STEADY-STATE OPERATING CONDITIONS Part 1 – Boiling Water Reactor

by

Ezddin HUTLI [1] ***and Ramadan KRIDAN*** [2]

[1] Institute of Nuclear Techniques, Budapest University of Technology and Economics, Budapest, Hungary
[2] Department of Nuclear Engineering, Faculty of Mechanical Engineering, University of Tripoli, Tripoli, Libya

Scientific paper
https://doi.org/10.2298/NTRP2204259H

The steady-state thermal-hydraulic analysis of the core of the Boiling Water Reactor (BWR/6) at nominal operating conditions is presented in this paper. The BWR/6 is produced by General Electric USA. The analysis' goal is to keep the thermal safety margin under control and the core integrity intact under steady-state operating conditions. The effects of operating conditions such as power distribution, power level, and coolant mass flow rate on the proposed core's performance are investigated. For this purpose, the one-dimensional computer code MITH was used. The code's reliability was tested using the General Electric benchmark 3579 MW reactor. Two-channel models were tested (the average and the hot channel). Thermal-hydraulic parameters such as fuel-centerline, fuel-surface, outer clad surface and coolant temperature, critical and actual local heat flux, critical and minimum critical heat flux ratio and pressure drop are evaluated along the tested channels. Temperatures, as well as actual and critical heat flux distribution profiles, were obtained. The tested operating conditions had a significant influence on these parameters, and also on the thermal-hydraulic performance. The obtained results are in good agreement with the data from the tested core. The obtained results are well within the safety margins. The good agreement between tested reactor data and MITH code calculation concerning the reactor demonstrates the reliability of the analysis methodology from a thermal-hydraulic perspective.

Key words: fuel, clad, coolant, power, heat flux, minimum critical heat flux ratio

INTRODUCTION

In the design steps of nuclear reactors, the analysis of the related experimental and calculation work is considered. Also, the analysis of nuclear accidents such as Three Mile Island, Chernobyl, and Fukushima (1979, 1986, and 2011 respectively) are reviewed and considered. The thermal-hydraulic analysis of light water reactors (LWR) cores is concerned with the thermal and hydraulic performance of nuclear fuel rod bundles. It includes several analysis topics such as pressure, core flow distribution, core void distribution, thermal margins (departure from nucleate boiling ratio (DNBR), critical heat flux ratio (CHFR), and fuel thermal performance) [1, 2]. The thermal-hydraulic and reactor physics analysis are assumed as the main tools used to ensure the safety of the nuclear reactor under different working conditions [3]. The sub-channel analysis codes for thermal-hydraulic analysis to estimate different thermal-hydraulic safety margins.

The coolant flow rate, inlet temperature, pressure, and thermal power and its distributions are considered as the main parameters for sub-channel analysis. The critical heat flux (CHF) is an important phenomenon „parameter" related to the operation of LWR, where cladding and core integrities must be maintained and a safe operating power envelope and margin must be established. The efficiency of nuclear reactors is limited due to the CHF phenomenon. It is essential for nuclear reactors not to reach CHF. The reactor's thermal design limits will be violated when the departure from nucleate boiling (DNB) occurs at full power, and the loss of fuel and cladding integrity is a result. CHF causes an increase in surface temperature due to a decrease in the heat transfer process. This temperature change can be fast, as is the case for pressurized water reactor (PWR) conditions *fast dry out*, or it can be slow as for boiling water reactor (BWR) conditions *slow dry out* [4]. Reaching and exceeding the CHF can have serious consequences, in particular for LWR. For this reason, CHF investigations became important since the mid 20 century, the earliest researches were done by McAdams *et al*. (1949), and Jens and Lottes (1951) [5, 6]. The long history and state of the art of measuring and predicting the CHF in

* Corresponding author, e-mail: ezddinhutli@yahoo.com

water-cooled systems are presented detailed in the literature [7]. The accurate estimations of the local conditions of the sub-channels are required to predict fuel temperature, CHF, DNB, CHFR, and critical power ratio (CPR) [1].

Currently, there are hundreds of empirical correlations to predict CHF. In the nuclear field, the CHF has a complex mechanism and different scenarios, thus no single correlation will ever be appropriate for every scenario. Many authors presented a comprehensive review of past, present, and future challenges in the field of thermal-hydraulic analysis, covering various aspects of experimental, analytical, and computational approaches [8]. The main factors affecting heat transfer from the fuel element are geometrical configuration, neutron flux distribution, types of fuel, gas gap and cladding used, and coolant flow conditions. In addition, the non-uniform heat transfer conditions influence the temperature and heat flux distribution in fuel and cladding [9].

To improve thermal-hydraulic characteristics of the nuclear reactor core, a considerable amount of research has been carried out to obtain an improved understanding of coolant flow and temperature distributions in rod bundle geometries. Many researchers have been worked in this field among them, Yadigaroglu *et al*. (2003) show the importance of both experiments and numerical simulation techniques to ensure the safety margin [10]. Chelemer *et al*. (1972) used the sub-channel analysis code to estimate the CHFR, CPR, temperatures of fuel (centerline, and surface), cladding surface, maximum temperature, and a bulk coolant outlet [11]. Cheng and Muller (2003) show that the maximum operating power of the reactor is limited by the CHFR, CPR, and fuel centerline temperature [12]. Helmy *et al*., (2012) investigated the thermal-hydraulic behavior of the KONVOI-PWR under design extension conditions. Their results show the importance of reactivity feed-back effects in loss-of-coolant accidents on the total power, which are considered as key parameters for controlling clad and fuel temperatures to keep them below their melting points [13]. Hutli and Kridan [14] investigated the effects of the axial power distribution on the main thermal hydraulics parameters in PWR using one dimensional sub-channel code [14]. Many other authors have demonstrated the dependence of CHF values on local fluid conditions such as pressure, temperature, mass flux, quality, and geometrical parameters [15-20].

The flow behavior in sub-channels under the two types of mixing process; natural and forced mixing was also a research point. The obtained results showed that, the mixing process strongly affects the local fluid conditions of the sub-channels, heat transfer coefficient, pressure drops and the outlet temperature profile of the core [21-25]. For single-phase, coolant reactors, the computational fluid dynamics (CFD) was used to estimate pressure loss, predicting the CHF rod position, and investigate the effect of spacer grade on CHF in a 5×5 fuel rod bundle [26]. The convenience of CFD modeling methodology and validation for steady-state flow in PWR fuel assemblies for the normal operation was investigated [27]. CFD analysis of the flow field in sub-channels of VVER-440 fuel assemblies for a triangular lattice was presented [28].

Because of the importance of the mixing process for heat transfer, reactor thermal-hydraulics, reactor performance, and reactor safety, many computational and experimental studies have been conducted using various techniques to investigate flow mixing behavior in normal and transient PWR and fuel assembly models (for single phase flow). The results of CFD, particle image velocimetry (PIV), and planar laser-induced fluorescence (PLIF) techniques revealed that the flow rate has a significant influence on the mixing process, and velocity and temperature distribution in the investigated area can be obtained, which are important parameters in determining thermal fatigue and pressurized thermal shock. Additionally, the results revealed that the inlet temperature is an important parameter for the PWR (for safety assessment) [21, 25, 29-31].

In the fluid flow field, two phase flow is considered complicated flow; as a result, designs of BWR core are complicated. Inside a BWR fuel bundle, two phase flow phenomena include coolant phase changes and multiple flow regimes that directly influence coolant interaction with the fuel assembly and, ultimately, reactor performance [32]. CFD is also used for thermal hydraulics analysis in BWR, with the CFD-BWR being developed to simulate two-phase flow phenomena inside a BWR fuel bundle. New models have been developed and implemented in the CFD-BWR module to describe the inter-phase mass, momentum, and energy transfer phenomena specific to BWR. The obtained results demonstrated that the good agreement between computed and measured results provides confidence in the accuracy of the models used [33].

For the two-phase flow condition, the TPFIT (two-phase flow analysis code with an advanced interface tracking method) was used to simulate steam-water two-phase flow in a model of two sub-channels from an actual BWR and Water Reactor for flexible fuel cycle core. The obtained result demonstrates that fluid mixing was detected between the sub-channels, that pressure difference between fluid channels is responsible for fluid mixing, and the inlet quality ratio of sub-channels is significant for the mixing process [34].

The thermal-hydraulic analysis for the steady-state operation of the BWR/6 core was performed in this work (GE) [32]. The motivation for this work is to establish the relationship between the various parameters influencing the thermal-hydraulic performance of BWRs. The typical reactor data of the tested BWR/6 is given in tab. 1. The MITH is a one-dimensional sub-channel computer code that is used to calculate the

Table 1. Typical nuclear power reactor data - BWR/6 (General Electric producer (GE)) [32]

General data	Value	Assemblies	Canned square bundles
		Assembly pitch [cm]	30.5
		Assembly dimension [cm^2] (Horizontal cross-section)	14 14
		Number of fuel /assembly	63
Thermal output [MW]	3579	Total number of fuel locations	46.116
Electrical output [MW]	1200	Fuel element O.D. [cm]	1.25
Efficiency [%]	33.5	Pitch/diameter	1.30
Fuel type	UO_2	Clad thickness [cm]	0.0864
Coolant	H_2O	Fuel-pellet diameter [cm]	1.056
Structural material	Zircaloy-2 alloy	Pellet-clad gap [cm]	0.008
Moderator	H_2O	Fuel enrichment	2.1/2.6/3.1
Core data			
Active height [cm]	376	Thermal-hydraulic data	
Equivalent\active diameter [cm]	366	System pressure (bar)	72
Height/diameter	1.03		
Active core volume	63.910	Coolant flow [10^6 kgh^{-1}]	47
Average core power density [kwL^{-1}]	56	Average linear power density [Wcm^{-1}]	206
Fuel weight [kg]	138.000	Maximum linear power density [Wcm^{-1}]	440
Specific power [kW/kgU]	25.9	Average heat flux [Wcm^{-2}]	50.3
Burnup [MWd/tU]	27.500	Maximum heat flux [Wcm^{-2}]	111.5
Conversion ratio (C.R.)	0.5	Minimum CHFR	1.9
Fuel assembly type	Canned-square bundle	Inlet temperature [°C]	269
Number of fuel assemblies	732	Outlet temperature [°C]	286
Fuel elementary array	8 8	Maximum fuel temperature [°C]	1829

associated thermal-hydraulic parameters. MITH is a steady-state code that was originally designed for PWR thermal-hydraulics analysis before being modified for BWR analysis. The analysis was done in two main steps. In the first step, thermal-hydraulic parameters such as the temperatures of fuel (centerline and surface), cladding, and coolant were calculated. Besides, the actual local heat flux, CHF, CHFR in the average, hot channels of the reactor core, and the core pressure drop were calculated. In the second step, the investigation of the influences of power distribution, and mass flow rate on the thermal-hydraulic parameters was done. For the code validation, the data of the GE typical BWR/6 reactor are considered as a reference, tab. 1. The code reproduced well the GE reactor results, yielding detailed information such as pressure drop in the channel, power distribution among the average and hot channels, coolant, clad and surface and centerline fuel temperatures, quality, actual local heat, and critical heat fluxes. The obtained results were compared with thermal design limits to determine the feasibility of the GE reactor core.

CODE DESCRIPTION

The code MITH is a thermal-hydraulic steady-state computer program. It calculates the coolant conditions (pressure, density, temperature, quality, *etc*.) and fuel rod temperature in both an average coolant channel and the maximum power coolant channel of LWR and also the actual local heat flux in both channels, also CHF and DNB in hot channels. In the MITH code, the application of the relations for conduction and convection would yield temperature profiles as shown later. The clad external surface, fuel centerline, and surface temperatures are obtained using certain related equations in conjunction with the coolant temperature distribution.

Three basic assumptions are made in formulating the problem to be solved by MITH. The first assumption that the channel flow in each coolant channel is constant and equal. An option is also available to equalize the pressure drop between the inlet and outlet of the two-channel by iteration on the flow in the max-powered channel. Thirdly it is assumed that the same axial power shape exists in an average and hot channel.

There are four axial power distribution options in MITH, the first three options require no additional input as they are computed using the following relations:

$$\text{Sine profile: } P(z) \quad P_o \sin\frac{z}{L}$$

$$\text{Bottom peaked profile: } P(z) \quad P_o \frac{(L \quad z)}{L}\sin\frac{z}{L}$$

$$\text{Top peaked profile: } P(z) \quad P_o \frac{z}{L} \sin\frac{z}{L}$$

Arbitrary profile is given as input the NAMELIST\ SHAPE.

In the code to avoid complexity, the entrance at the bottom of the channel is assumed as a reference point ($z = 0$) for the calculation, therefore the sine function is used instead of the cos function, however the cos function is usually used in literature when the zero point is assumed at the medial of the channel. Option number four is used when the control rods are involved. Option number 2 is more convenient for BWR.

Finally, it is assumed that to the extent that the above assumptions are valid, one can define a limiting power generation for anyone channel the operator must then maintain the power distribution such that no channel exceeds this limit. The hot channel factor represents the ratio of the maximum to average channel power generation is an input parameter. Figure 1 (a) and 1(b) represents the flowchart of the code and the channel model respectively. Because the code was originally designed for PWR (single-phase), enthalpy was not a logical option while the vapor quality is calculated by the code, so coolant temperature profiles will be presented even though temperature is not a good indicator of the coolant's heat content in a two-phase flow. The enthalpy profiles that will be presented later are calculated manually using thermodynamic tables based on the coolant temperature and vapor quality along the channel length. For the same reason, the CHFR is used instead of CPR, and the GE-correlation was added to the code algorithms to calculate the CHF at high vapor quality, as in the case of BWR. Figure 2 depicted the schematic diagrams of the typical axial power profiles (relative power as function of the sub-channel axial nod) [35].

CODE INPUT DATA

The input data are; thermal power output (MW), mass flow rate [kgh^{-1}], coolant inlet temperature [°C], inlet pressure [bar], number of fuel rods, the outer diameter of fuel rod [cm], clad thickness [cm], unheated upper channel part [cm], unheated lower channel part [cm], pitch type, rod pitch [cm], active channel length [cm], number of a discrete interval, the form factor for spacer grids, profile power distribution, and radial num-

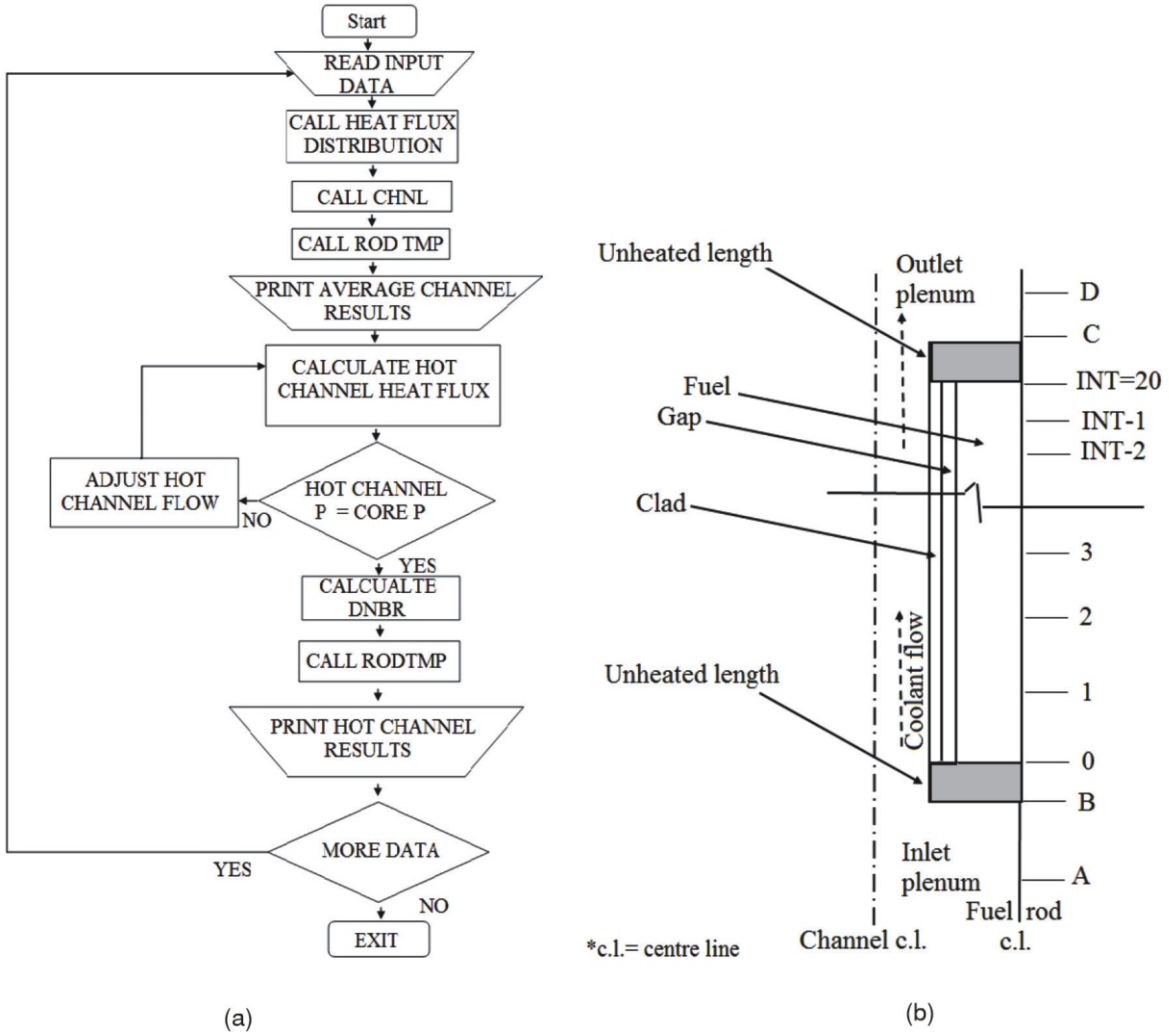

Figure 1. Flowchart of the code (a) and channel model (b)

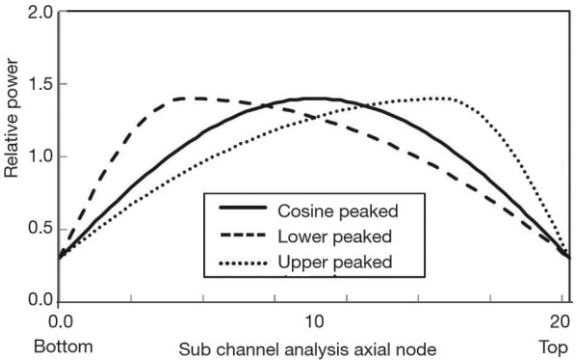

Figure 2. Schematic diagram of the typical axial power profiles [35]

ber hot channel factor. Also the thermal conductivity of fuel UO_2 (0.0294 $Wcm^{-1}°C^{-1}$), the thermal conductivity of clad zircaloy-2 (0.164 Wcm^{-1} $°C^{-1}$), and the heat transfer coefficient of the gas in the gap helium (25.94 Wcm^{-1} $°C^{-1}$).

METHOD

The present analysis has been implemented for the core of a typical nuclear reactor with specifications presented in tab. 1. GE Boiling Water Reactor (BWR/6) Model 6 Reactor Vessel produced by General Electric Company (GE, USA).

The effect of the power distribution on the reactor thermal-hydraulics has been investigated using the computer code (MITH) and the results are analyzed. The effects of an operating power level and the reduction in the coolant mass flow (the fraction of the total mass flow rate) on the core thermal-hydraulic performance and parameters have been also studied.

The calculation and analysis of the obtained results have been carried out for steady-state operating conditions under the following situations:

- Axial power distribution is symmetric around the midplane of the core.
- Axial power distribution is peaked below the core midplane (bottom peaked distribution).
- Increasing and decreasing the operating power level.
- Decreasing the coolant mass flow rate.
- Variation of operating power level and coolant mass flow with the same percentage of their nominal values.

RESULTS AND DISCUSSION

Influence of power distribution

To show the dependency of the thermal-hydraulic parameters on the axial power distribution in core two typical axial power distribution profiles have been tested. As the sinusoidal power is often used for conservatism, the sinusoidal axial power distribution is introduced as the first power profile to be tested, and then the bottom peaked power distribution as the second tested profile. The typical shapes of reactor power profiles are in fig. 2.

For the sinusoidal peaked power profile, the axial power was shaped as a cosine function as that in fig. 2, with $q(z)$ $q_{\max}\cos(z/H)$ the power is distributed symmetrically around the center of the fuel with the maximum power value is at the center. To achieve this kind of power distribution, the control rods are used to modify the neutron flux distribution. However, the second case (bottom peaked power profile) is easier to achieve in the LWR. The BWR have a significantly bottom-peaked axial power profile rather than the other power profiles. The BWR have a natural tendency to power shaping skewed toward the bottom because of the gradual boiling of the coolant. The boiling means decreasing in water density and increasing in both quality and void fraction with the elevation, thus the power generation will be higher in the lower part of the core than the upper part because the moderation of the neutron flux is greater in this part, more explanation is provided in the following sections.

COSINE PEAKED POWER DISTRIBUTION

The coolant temperature in the average channel

Coolant enters the bottom of the core, flows upward around the fuel rods, and absorbs energy from heat transfer originating from the nuclear process in the fuel element. In fig. 3(a) the profile shows that the coolant temperature started to increase as the coolant enters the channel, arrives at its peak at a certain distance along the channel, then becomes a constant to the channel end (core outlet).

In the case of BWR, the steady-state operating system pressure is low to allow the boiling process to be faster, and the inlet coolant temperature is not much lower than the saturation temperature of the applying pressure as it is presented in reactor data, tab. 1. In the BWR the upward coolant flow leads to temperature increase with the height, hence quality and void fraction increase with the height.

The recorded coolant temperature at the channel inlet and outlet was 268.9 °C and 287.64 °C respectively. The difference between inlet and exit temperature was recorded as an 18.74 °C. The obtained outlet temperature represents the saturation temperature for reactor operating pressure (72 bar). According to the thermodynamics principles, after the point where the coolant phase started to change, any increase in the heat does not lead to an increase in the coolant temperature. The gained heat from the source is consumed to complete the phase change process; hence, quality and

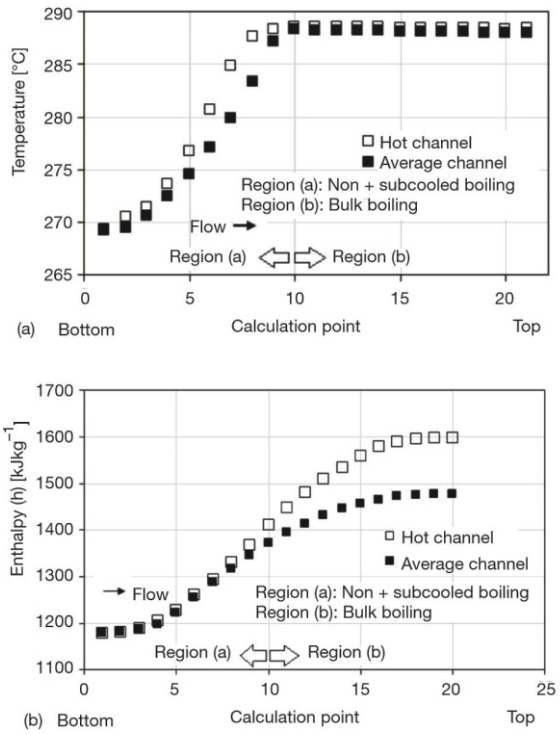

Figure 3. (a) Coolant temperature distribution in the average and the hot channel and (b) Coolant enthalpy distribution in the average and hot channel (steady-state operation at nominal power (cosine peaked power distribution)

void fraction are increased as in fig. 6(c). (Figure 6(c) is for bottom-peaked case). After the coolant liquid phase completely changed to the vapor phase, the temperature again starts to increase and we will have the superheated vapor.

According to reactor physics, we assumed that the cosine peaked power distribution is not realistic in a BWR reactor. The cosine peaked profile is used in this study to compare the effect of axial power distribution shape on thermal-hydraulic parameters.

The core reactivity and core power are affected locally and globally as a result of a significant drop in coolant density with elevation in the core. The variation of coolant density affects the neutron flux spectrum because the neutron moderation process decreases as density decreases, affecting power produced per unit length of fuel rod. The presence of voids shifts the power toward the core's bottom; the voids increase with the magnitude of the peak and as the peak moves toward the core's bottom. Similarly, the BWR has an inherent capability of self-flattening the radial power distribution due to changes in coolant density [36]. Also, for precise thermal-hydraulic analysis, the density waves in the boiling region which normally exists should be considered because it leads to flow oscillations. The flow oscillations can affect the local heat transfer characteristics. It may induce burnout, cause mechanical vibration of components; and create system control problems [37]. Regarding the previous discussion, for a continuous heat removal process from the core, the coolant should be physically and chemically stable under high temperature and nuclear radiation, which is well considered in the LWR design [36, 38].

Generally, in the boiling channel flow such as that in BWR, the coolant temperature rises as the heat is transferred to the coolant with the distance (vertical or horizontal flow), the distance after the temperature saturation occurs, and coolant bulk boiling begins is called boiling length. The distance before the coolant temperature is started to change from sub-cooled to the saturation temperature (bulk boiling begins) corresponding to the operating core pressure is assumed as non-boiling length (we assuming that the sub-cooled boiling length is a component of non-boiling length). In BWR these distances are important for the calculation and estimation of some thermal-hydraulic parameters such as quality, void fraction, heat transfer coefficient, CPR or CHFR, power peak shape, pressure drops, *etc*.

The coolant temperature in the hot channel

In the design of a reactor, a great deal of attention is given to the determination of which channels have the highest coolant temperature and at which points on the fuel rods hot spots occur. The hot channel is defined as the channel that recorded the highest temperature of fuel, cladding, and coolant in the reactor under steady-state operating conditions. The other channels in the reactors have temperatures lower than that of the hot channel. Therefore, when the hot channel satisfies the thermal limiting conditions, means the other channels are well with the safety limits. Hence the hottest channels are considered as the indicator of the preservation of safety margins. Ultimately, the power of the reactor is limited by conditions at these channels.

The coolant temperature profile in the hot channel is presented in fig. 3(a) has the same shape and behavior as that in the average channel. The difference is in the ratio between the lengths of boiling and non-boiling length, it is smaller in the hot channel. In the hot channel, the coolant reaches the boiling point after a short distance *short length* and faster *time*, which is related to the difference between the heat generation levels in the two channels. The outlet temperatures are equal in both channels; it's a saturation temperature of the core operating pressure. One can say that, under the assumption of constant operating pressure and the equal mass flow rate in the channels, the ratio between boiling and non-boiling length and the time needed to start boiling is depending on many other factors such as the inlet coolant temperature, the axial power distribution, and power level generated within the channel.

Because the coolant is changing its phase, the coolant temperature profile is not altogether descriptive of coolant energy increase. To describe the status pre-

cisely the enthalpy change must be utilized. The coolant enthalpy continuously increases from core inlet to outlet, with the largest rate of increase at the maximum value of heat flux [39]. Because the code was mainly for PWR calculations, the variation of the coolant enthalpy with elevation was not calculated by the code. To describe the heat transfer status precisely the enthalpy change was utilized. The coolant enthalpy profile for both average and hot channel are presented in fig. 3(b). The presented results in fig. 3(b) were calculated manually based on the quality distribution along the channels which is calculated by the code, as in fig. 3(b) we assumed that the sub-cooled boiling region is a component of the non-boiling region (region (a), because determining the boundary between the non-boiling region and the subcooled boiling region in the channels is difficult. This assumption can be accepted if one considers that, the thermal hydraulic analysis done here is for BWR where the bulk boiling is necessary feature, while in the sub-cooled boiling region the vapor quality is not measurable value (it is very low). The temperature of the most of the liquid (bulk temperature) in the subcooled boiling region *process* is below the saturation temperature, and bubbles formed at the surface condense in the liquid. Then region (a) is extending from the channel's inlet to the region where the coolant's bulk temperature reaches the saturation temperature of the applied pressure (region (b). Figure 3(a) are used to approximate the border between these two regions (region (a) and region (b)).

Sub-cooled boiling may occur in this region. The analysis of fig. 3(b) reveals that the enthalpy continuously increases from the channel inlet to the outlet. At the channel inlet, the enthalpy was constant, which was equal to the enthalpy of the saturated subcooled water. While by starting the boiling process and change of the phase, the increase in the heat transfer to the coolant will appear as an increase in the coolant enthalpy. As the bulk boiling begins, the enthalpy continues to rise until it reaches its peak at the channel outlet. The enthalpy profile behaves oppositely compared with the coolant temperature profile. The amount of heat generated in any channel in the reactor core can be indicated by coolant temperature in the non-boiling region of the channel (assuming sub-cooled boiling region is a part of the non-boiling region), whereas coolant enthalpy is a more reliable indicator in the boiling region (bulk boiling region) of the channel.

Clad, fuel-centerline, fuel-surface temperature in the average, and the hot channel

The tested reactor's cladding material is strictly defined in the datasheet [32]. It is zircaloy-2, which is commonly used in BWR (zircaloy-2 (Grade R60802) is composed of Zr-1.5 %, Sn-0.15 %, Fe-0.1 %, Cr-0.05 % Ni). Zirconium alloys serve as the structural material because they have excellent properties for use as fuel cladding and other structural materials in nuclear reactors. Zirconium is a commercially available refractory metal with excellent corrosion resistance, good mechanical properties, and very low thermal neutron cross-section, and can be manufactured using standard fabrication techniques [40]. Also, the tested reactor's fuel material is strictly defined in the datasheet [32]. The fuel is uranium dioxide (UO_2), it is a ceramic refractory uranium compound, in many nuclear reactors used as a nuclear fuel. It is a stable ceramic that can be heated almost to its melting point (2878 20 °C), without significant mechanical deterioration. It has no significant reaction with water [41].

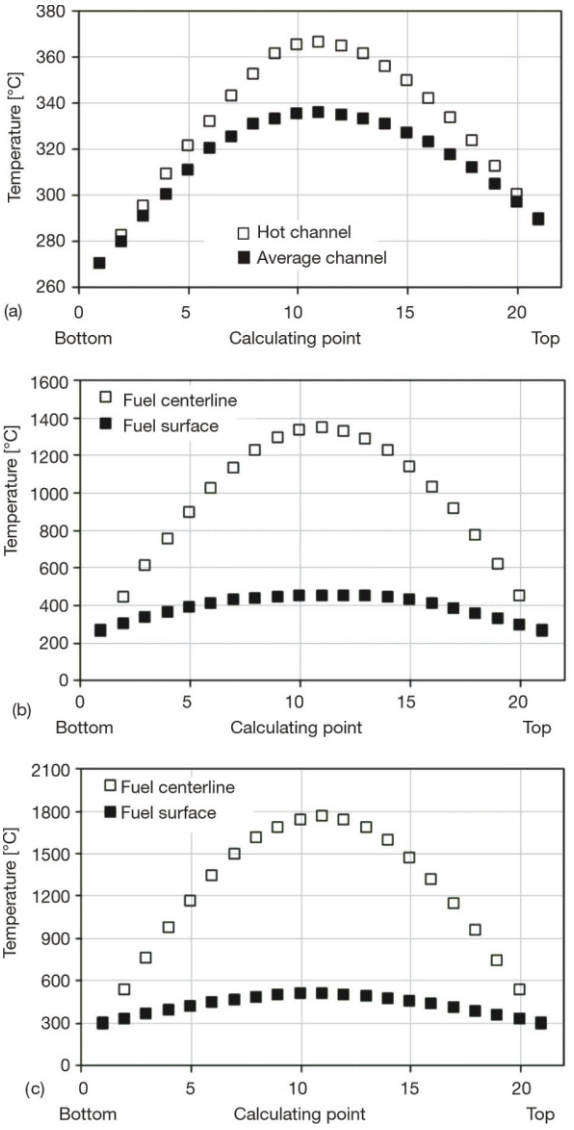

Figure 4. (a) Axial temperature distribution in the cladding (average and hot channels, (b) Axial temperature distribution in the fuel in the average channel, and (c) Axial temperature distribution in the fuel in the hot channel (steady-state operation at nominal power, cosine peaked power distribution)

In fig. 4(a) the cladding axial temperature profiles for the average and the hot channel are presented.. The analysis of fig. 4(a) shows that the cladding temperature for average and hot channels increases with distance arriving at its peaks 335.41 °C, and 367.7 °C respectively, approximately at the half of the fuel element *half of the channel*. Where the channel inlet is assumed as a reference point. Then it starts to decrease slowly with distance reaching the outlet coolant temperature 287.64 °C at the top of the channel. The obtained profile follows the applied power distribution in the core (it is assumed that at the channel ends the power is zero). The dissimilarity between the clad and coolant temperature profiles is related to many reasons such as the clad is near to the heat source (fuel) compared with the coolant, the heat capacity of the coolant, and other thermal properties for both cladding and coolant, also the coolant is moving while the clad is stationary. Regarding the safety point of view, the clad maximum temperature recorded in the hot channel under these working conditions is still below the thermal limit, it is less than the melting temperature of the clad.

Figure 4(b) shows the axial temperature distribution in the fuel-centerline and fuel surface in the average channel. The centerline-fuel temperature profile shows that the temperature is increasing gradually reaching the maximum temperature of 1340.56 °C nearly at the medial of the channel *Fuel element*, and then decreasing gradually again to reach the minimum temperature at the end. The surface-fuel temperature profile shows the same behavior as the centerline-fuel temperature profile. The maximum temperature recorded on the fuel surface is 447.37 °C. The highest temperatures of the fuel centerline and fuel surface occur at the center of the fuel element axial length. Thus, the obtained temperature profiles have a similar shape as that for the applied power distribution *i. e*. the symmetric profiles are established. The difference between the two profiles in fig. 4(b) is related to the heat generation rate in the fuel pin itself. Also, the fuel surface is the nearest to the coolant.

Figure 4(c) presents the axial temperature distribution in the fuel-centerline and fuel surface in the hot channel. The temperature profiles in the hot channel presented in fig. 4(c) are similar in shape and behavior to that in the case of the average channel, which is related to the applied power distribution. Generally, in the hot channel, the fuel centerline, fuel surface, and clad surface temperature profiles are higher than that in the average channel. The difference between the hot and average channels in the temperature levels of the fuel element is related to the big difference in the heat generation in the two channels as mentioned earlier. In the hot channel, the maximum temperatures recorded at the centerline fuel and the fuel surface are higher at 1756.98 °C and 507.23 °C, respectively. Regarding the safety point of view, the maximum temperatures in the hot channel under these working conditions are still below the thermal limit. Because of the assumption of zero neutron flux at the bottom and the top of the channel the temperature of the fuel, the clad, and the coolant are equal at these two ends.

CRITICAL, LOCAL HEAT FLUX AND MCHFR

In the nuclear reactors, the steady-state power should be kept at levels that allow margins to prevent CHF conditions. The CPR in BWR reflects the CHF, which is the ratio of the CHF to the actual heat flux of a fuel rod. While CHF is reflected in PWR by the DNBR, which is the ratio of the CHF (the heat flux required to cause DNBR) to the local heat flux of a fuel rod. These ratios take into account the phenomenon's margin [42].

The margins should be enough to allow for expected operational incidents. The ratios between critical and actual parameters have many forms such as a minimum critical heat flux ratio (MCHFR), minimum departure from nucleate boiling ratio (MDNBR), a minimum critical channel power ratio (MCCPR), and a minimum critical power ratio (MCPR). These ratios are much considered in the design of water-cooled reactors.

The CHFR is used here instead of CPR for three reasons: first, the code was originally written for PWR, and the algorithms for calculating CPR do not exist in the code; second, the MCHFR is given instead of MCPR in the data sheet of the tested reactor (tab. 1); third, the CHFR is more convenient for plant safety evaluations than the CPR, because CHFR values can be determined at reactor operating power, whereas CPR computation requires a search for the critical power level [43]. As mentioned in the literature, The MCPR, which is used as a limit to avoid the occurrence of the dry-out phenomenon, has a corresponding value of MCHFR. Typical thermal design limits presented by US Nuclear Regulatory Commission (NRC) stated that, MCPR 1.2 is the limit for BWR at 100 % power, and its corresponding minimum critical heat flux ratio is approximately1.9 [44]. It was also stated that the design basis for water-cooled reactors is a MDNBR of 1.3 [45].

The CHF which limits the heat transfer capability of boiling systems, and the actual local heat flux are calculated. Two CHF correlations were employed in the code (GE and W-3 correlations).

The calculated heat fluxes are presented in fig. 5. The hot channel shows a higher actual heat flux compared with the average channel (curve 1 and 2 in fig. 5 respectively) are presented to show the reader the difference between the channels. This difference is related to the hot channel factor (power generation in each channel). The curve 1 and curve 2 in fig. 5 appears as identical at the core end points (bottom and top). It does not mean that the two channels have the same value of heat flux at their ends, but the drawing scale displays them as equal. Because the hot channel

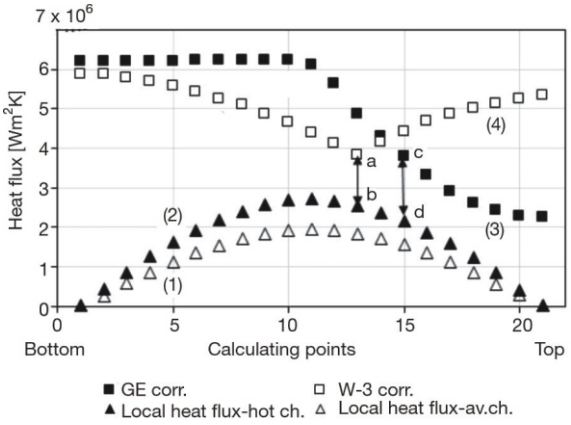

Figure 5. Axial profile of critical and local heat flux distribution in the hot and average channel (steady-state operation at nominal power (cosine peaked power distribution)

parameters are used to calculate CPR, the hot channel must be considered in concepts of reactor safety.

Curves 3 and 4 are CHF profiles along the channel *fuel element* calculated using GE and W-3 correlations, respectively.

Curve 3 shows that the CHF obtained using GE correlation appears as a constant value with height for the distance approximately half of the channel *fuel element*. in the real it is not a constant, but the variation of CHF is small in the first half of the channel, this variation cannot be presented because of the used scale. After the first half of the fuel element, the CHF starts to decrease gradually. This is due to the start of the phase change process, which results in an increase in vapor quality. As a result, the film vapor will cover the surface (partially or completely) and the heat transfer rate in that region will decrease. The line cd between curve 2 and curve 3 represents the position of the minimum ratio between the CHF and the local actual working heat flux MCHFR. At that position the MCHFR is 2.024. The obtained MCHFR value is under the safety margin proposed by safety regulation and design [44]. MCHFR position could be used as an indicator to determine the point at which the melting phenomenon in fuel and clad could occur. Therefore, the area within the MCHFR value has a higher probability of fuel damage compared to the other areas in the fuel element itself. Generally, because of the higher local heat flux in the hot channel compared with other channels in the core, the higher probability of fuel damage will be in the hot channel.

Curve 4 (W-3 correlation) represents the obtained CHF profile obtained using the W-3 correlation. The CHF profile shows that CHF is not constant, it decreases slowly with a distance from the bottom and then after approximately 70 % of the channel length *fuel element length* starts to increase with the height. The line ab between curve 2 and curve 4 represents the position of MCHFR. At that position the MCHFR is 1.77, *i. e.*, the obtained value of MCHFR is under the safety margin proposed by safety regulation and design. There is a clear difference between the two profiles of CHF (curves 3 and 4). The variation in the shape of profiles and their behavior leads to a difference in MCHFR values (2.024 for GE and 1.7 for W-3) and MCHFR position along the channel.

The differences in the value and the position are related to the validity of the W-3 for the reactor operating conditions and limitations such as pressure, temperature, and coolant conditions. Among the coolant conditions is the vapor quality x, the W-3 correlation is valid for x 0.15 in the hot channel.

Even though the W-3 result is within the design basis for water-cooled reactors (MDNBR or MCHFR) it does not meet the design limits presented by the designer of the tested reactor (tab. 1)[32]. Because the vapor quality is greater than the W-3 correlation application limit (vapor quality limit) the CHF profile produced by the W-3 correlation will be deceptive in terms of MCHFR value and position of the dray out phenomenon. Because the vapor quality is higher in BWR; x 0.2, the GE correlation was incorporated to the code, making it more suitable for BWR operating conditions.

BOTTOM PEAKED POWER DISTRIBUTION

The coolant temperature in the average and the hot channel

The coolant temperature in the average and hot channels are presented in fig. 6(a). Analysis of the profiles in fig. 6(a) reveals that, in both channels, the coolant temperature starts to increase gradually with height until it has arrived at its peak of 287 °C at a certain point before the half of the channel. The 287 °C represents the saturation temperature of the operating pressure. The temperature profiles have the same behavior. The difference between the two channels is in the distance that needed to be traveled by the coolant to reach the saturation temperature where the phase change started. In the hot channel, the non-boiling distance is less than that in the average channel, thus the time needed to start the phase change process in the hot channel is lower. Therefore, in the hot channel, the ratio between the boiling and non-boiling distance along the channel is bigger. The reason is related to the hot channel factor (power level) because of the variation of their positions in the core. Figure 6(b) represents the coolant enthalpy profiles, the comments provided for fig. 3(b) are valid for fig. 6(b). The large step of the abrupt increase in the enthalpy value in fig. 3(b), which is not seen in fig. 6(b), is due to the applied power distribution. To understand the whole process and the mechanism of the heat transfer in the channel

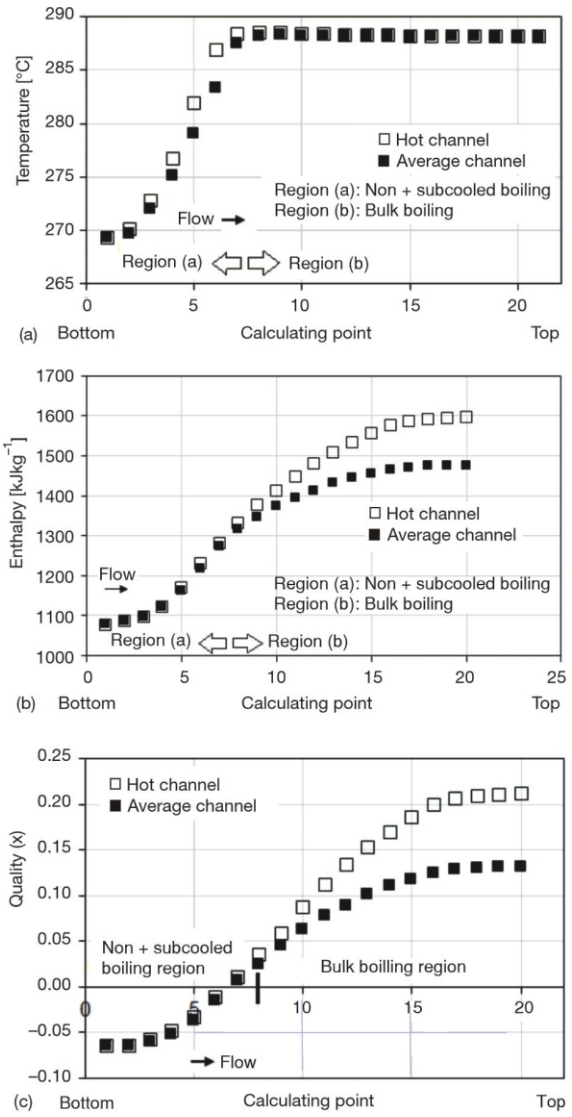

Figure 6. (a) Coolant temperature distribution in the average and the hot channel, (b) Coolant enthalpy distribution in the average and hot channel, and (c) Variation of the quality along the channel in both channels (steady-state operation at nominal power (bottom peaked power distribution)

from the fuel element to the coolant figs. 6(a) and 6(b) should be considered. As it is mentioned earlier the ratio between the non-boiling and boiling regions depends on many factors. Since here only power distribution was changed, compared with the previous case (cosine distribution) the ratio of the boiling to non-boiling distance is bigger in this case. Also, the time which is needed to start the boiling process is expected to be smaller, *i*. *e*. the boiling starts faster. This can be deduced by the comparison between figs. 3(a) and 3(b) and figs. 6(a) and 6(b). Figure 6(c) shows the variation of the quality with the length, the non-boiling part is presented by negative quality values while when the bulk boiling is started the quality will have positive values. We have to notice that, before the boiling process starts there is no phase change happen therefore the negative values of the quality that appear in fig. 6(c) are misleading and could be used as a good indicator for the non-boiling length of the channel. Also, the quality profiles show the difference between the hot and the average channel. Figure 6(c) is given here just as a piece of evidence for the difference in the heat generation level in both channels and also to show the variation of the coolant density with length.

Clad, fuel-centerline, and fuel-surface temperature in the average and the hot channel

Figure 7(a) presents the distribution of the clad temperature in the fuel elements in the average and hot channels. The analysis of fig. 6(a) reveals that in both

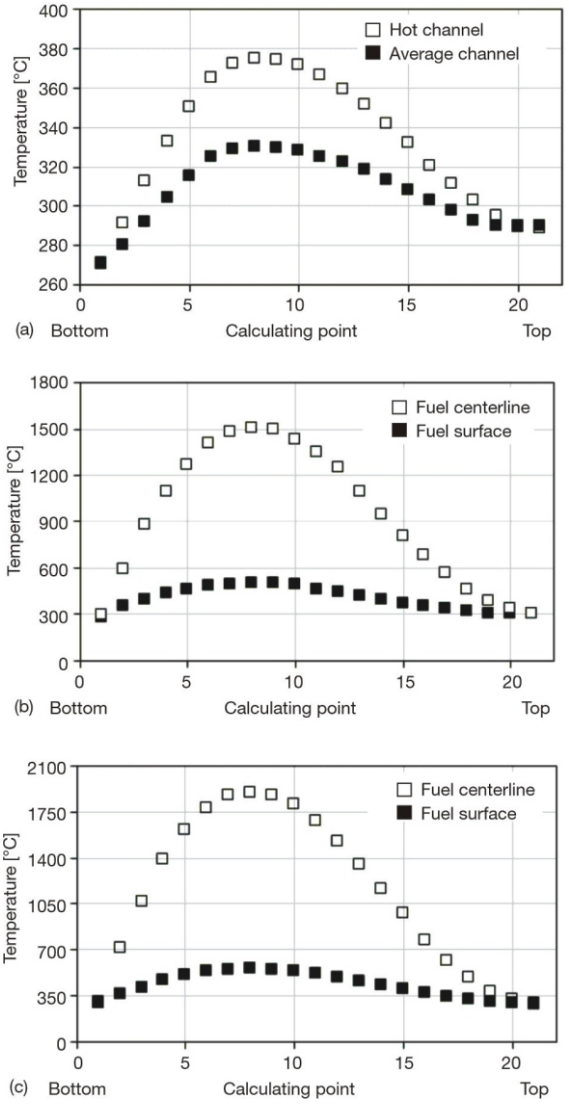

Figure 7. (a) Axial temperature distribution in the cladding (average and hot channels), (b) Axial temperature distribution in the fuel in the average channel, (c) Axial temperature distribution in the fuel in the hot channel (steady-state operation at nominal power (bottom peaked power distribution)

channels (average and hot) the cladding temperature increases with height arriving at the maximum values (330.09 °C and 378.7 °C, respectively) then decreases gradually arrived to value near the outlet coolant temperature T_{out}. The position of the maximum temperature in the clad surface is recorded at the distance before the half of the channel (fuel element). The difference in the position of the two channels is a reason for the big difference between the obtained profiles. The clad temperature distribution in both channels is similar to the applied power distribution. The temperatures of cladding and the coolant at the inlet and outlet are matched this is because of the applied power distribution as mentioned earlier (the power is zero at the channel ends).

Figure 7(b) shows the temperature profiles at the centerline fuel and fuel surface in the fuel element in the average channel. The fuel centerline temperature profile shows that the temperature increases gradually with the distance arrived at its maximum (1507.52 °C) at the distance before the half of the channel, then decreases gradually with the distance arrived nearly to the outlet coolant temperature (287.64 °C). While in the case of the fuel surface, the temperature profile has the same shape and behavior as that for the centerline, but the maximum temperature recorded along the fuel surface is much lower (499.25 °C). The two profiles have a similar shape as that for the applied power distribution (bottom peaked). Two profiles matched the coolant temperature at the inlet and outlet. Figure 7(c) shows the obtained profiles of the centerline and surface fuel temperature in the fuel element in the hot channel. The profiles have the same shape and behavior as that of the applied power distribution, fig. 2. The temperature profile at the fuel-centerline shows that the temperature increases gradually reaching its maximum temperature (1896.49 °C) at a certain point before half of the fuel axial height, then decreases gradually with distance reaching the outlet temperature of the coolant. The temperature profile at the Fuel surface has a similar tendency to that for the fuel-centerline, but generally, the recorded temperature on the fuel surface is lower, thus the maximum temperature recorded on the fuel surface is much lower compared with that in the fuel-centerline (551.11 °C). Figures 7(a)-7(c). 7(c) show that at the channel inlet and outlet, the centerline, fuel surface, and clad temperature are matched the coolant temperature the reason is mentioned early.

Critical, local heat flux, and MCHFR

The obtained heat fluxes are presented in fig. 8, Curve 1 and 2 represent the actual heat flux q''_{actual} distribution in the average and hot channel respectively. Even fig. 8 shows that the curves are identical at the channel inlet and outlet, the used scale showed them equally because the difference is not big at these ends

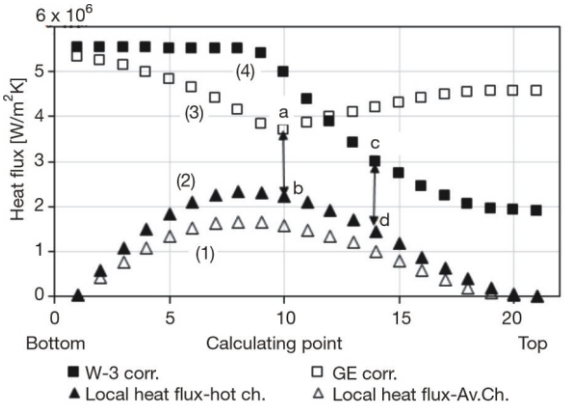

Figure 8. Axial distribution of critical and actual local heat flux in the hot and average channel (steady-state operation at nominal power, bottom peaked power distribution)

point, while as we moved from both sides toward the center the difference is increase with distance. For both average and hot channel, the maximum value of q''_{actual} recorded at the same position where the maximum fuel and clad temperatures were recorded.

As in Curve 4 (GE correlation), The obtained CHF appears as constant values from channel inlet to a certain distance along with the fuel element, because its variation is small in the first half of the channel, again the reason is the used scale. Approximately, after the first half of the fuel element, the CHF starts to increase gradually, as it is over mentioned. The line cd represents the position of the minimum ratio between the CHF and the local heat flux (MCHFR). The MDNBR 1.99. The obtained value of MCHFR is will with the limit proposed by safety regulation and design.

In Curve 3 (W-3 correlation), the obtained CHF profile shows that the CHF decreases gradually with distance from the bottom and then begins to increase gradually with distance after approximately half of the channel length. The line ab represents the position of the minimum ratio between the CHF and the local heat flux (MDNBR). The MCHFR is 1.50.

The clear difference between GE and W-3 correlations could be noticed from the shape of the obtained CHF profiles and their behavior (curve 4 and 3). This difference leads to a difference in the values of MDNBR (1.99 for GE and 1.50 for W-3) and their position along with the fuel element, the reason is mentioned above. The comments made about the results of the W-3 and GE correlations in the case of cos power peaked are also acceptable here.

The comparison between fig. 5 and fig. 8 shows the influence of power distribution on the actual and CHF hence on MCHFR value and its position in the fuel element. Therefore, the power distribution is an important parameter for thermal-hydraulic analysis, design, and determination of the thermal limits for cladding and fuel *i. e*., the overall thermal-hydraulic performance.

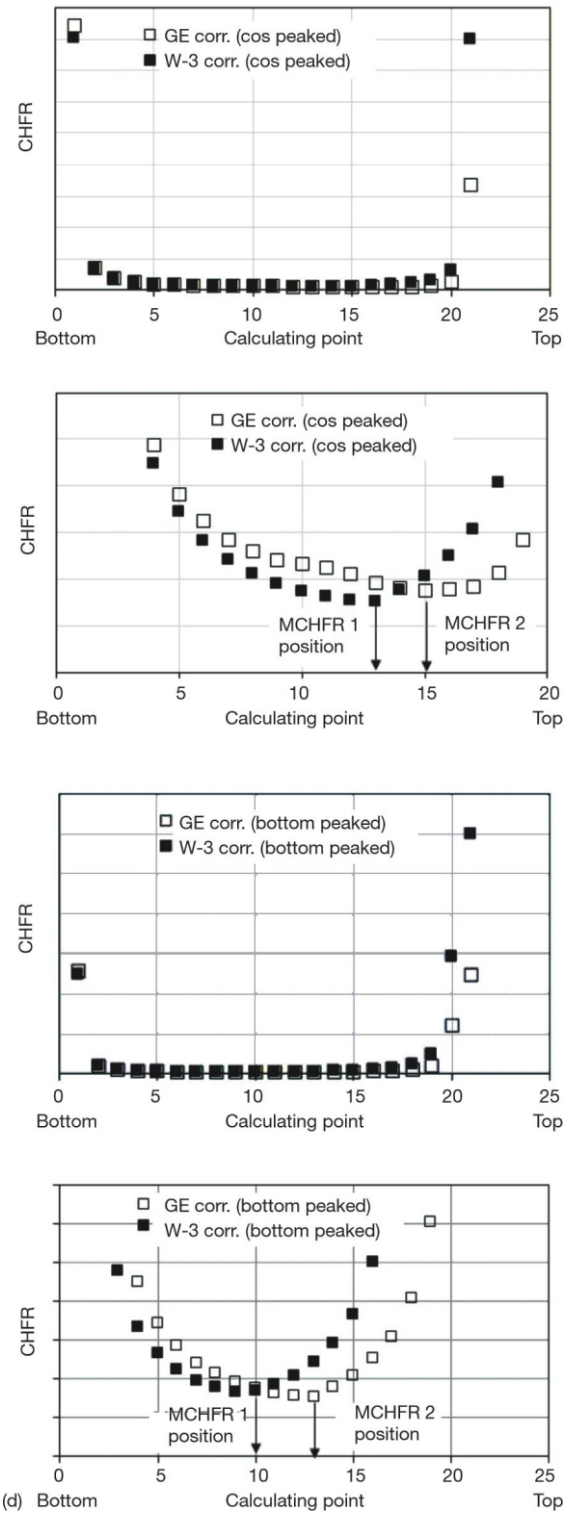

Figure 9. Influence of axial power distribution and the applied correlation on CHFR distribution in the hot channel; (a, b) CHFR in cosine peaked power distribution case; (c, d) CHFR in bottom, peaked power distribution case ((b) and (d) are anlarging the bottom parts of the CHFR curves in (a) and (c), respectively)

The dependency of CHFR distribution and MCHFR position on the power distribution and the correlation used for calculating the CHFR can be deduced from fig. 9(a,c) and fig. 9(b,d) respectively. Because of the effect of increasing fluid enthalpy on decreasing CHF, the minimum occurs downstream from the maximum heat flux position (fig. 5, fig. 8, and fig. 9(b,d). Because of the high vapor quality is created in BWR, the GE correlation result is more reliable than the W-3 correlation result.

Table 2 is introduced to relays the influence of the power distribution on maximum fuel, cladding, coolant temperature, and MCHFR values. Also, the data of the reference reactor is introduced to see the deviation of the obtained results.

INFLUENCE OF FLOW RATE AND POWER VARIATIONS ON TEMPERATURES AND MDNBR VALUE

The investigation of the influence of the power and the mass-flow variations on the fuel (center and surface) and cladding temperature and MCHFR was done for two cases under the assumption of steady-state reactor conditions. In the first case, the power and the coolant mass-flow rate were changed by the same percentage regarding their nominal values tab. 1. In the second case, the power was changed and the mass flow rate was kept constant. The temperatures and MCHFR were calculated under those conditions.

Table 3 represents the obtained result of the first case. The results revealed the temperatures are decreasing in both average and hot channels when the power and mass-flow rate are decreasing with the same percentage, however, the MCHFR is increasing. This is because the decrease in the power using control rods or other absorbers leads to a decrease in fission reaction rate in fuel, *i.e. the thermal power generation from the fuel decrease* hence the clad temperature will decrease and the actual local heat flux decrease as consequence. It is also true when the mass-flow decrease, the coolant density is changed faster, leading to a decrease in the moderation rate, therefore the fission reaction rate will be decreased *i. e.*, power generation decreases, hence the actual heat flux decreases. While under the assumption of constant core operating pressure, the coolant temperature stays a constant equal to the saturation temperature as the phase change is started as mentioned earlier. It is expected that the variation of power and the mass-flow rate have an influence on the boiling and non-boiling region *distance along channel* and time needed for the coolant to reach its maximum temperature *saturation temperature* of the operating pressure. It should be noted the power level can be increased during normal operation easily by increasing the coolant flow rate. Thus, the steam will be decreased in the core giving greater moderation and a higher thermal neutron flux. The increased heat output causes more steam to be produced, and the reactor settles down to a new, higher, power level [38]. The small difference that appears in saturation temper-

Table 2. The influence of power shape on the maximum temperature of the fuel center line and the clad outer surface in the hot channel, as well as the MCHFR value

Parameter	Power distribution		Tested reactor	Melting temperature [°C]
	Cosine peaked	Bottom peaked		
Coolant temperature [°C] (average channel)	287.64	287.64	286	
Clad maximal temperature [°C]	367.173	378.7	–	1850 °C [39]
Fuel centerline temperature [°C]	1756.98	1896.49	1829	2878 20 °C [40]
MCHFR	2.024 (GE) 1.77 (W-3)	1.992 (GE) 1.501 (W-3)	1.9	

Table 3. Influence of variations of flow rate and power on temperatures and MCHFR (bottom peaked)

Flow rate	Power	Average temperature [°C]			Maximum temperature [°C]		MCHFR
		Coolant	Clad	Fuel-centerline	Clad	Fuel-centerline	
115	115	287.15	390	1776.94	391.3	2235.43	1.5921
100	100	287.18	330.9	1507.52	378.7	1896.49	1.99
85	85	287.20	302.4	1377.84	366.1	1733.27	2.5323
70	70	287.23	258.1	1175.99	353.4	1479.35	3.0038
50	50	287.26	199.0	906.79	336.5	1140.70	3.0917
25	25	287.28	125.1	569.99	370.5	717.03	7.1138

Table 4. Influence of variations power on temperatures and MCHFR at a nominal operating flow rate (bottom peaked)

Flow rate [%]	Power [%]	Average temperature [°C]			Maximum temperature [°C]		MCHFR
		Coolant	Clad	Fuel-centerline	Clad	Fuel-centerline	
100	115	287.15	390	1776.94	391.2	2241.05	1.29
	100	287.18	330.9	1507.52	378.7	1896.49	1.99
	85	283.82	305.0	1377.84	366.11	1733.3	2.7
	70	283.31	258.1	1175.99	353.38	1479.31	3.3129

ature recorded values could be related to the accuracy of the code. Table 4 represents the results of the second case, in this case, the power was changed and the mass-flow rate and operating pressure were kept constant, decreasing in the power level leads to a decrease in the temperature in the average and the hot channel and increasing in MCHFR values, the reason is over mentioned.

Figure 10(a) and fig.10(b) graphically show the influence of both power level and mass flow rate on the fuel, clad temperatures, and the MCHFR respectively at steady-state operating conditions. The influence of the power level was tested at 100 %, 75 %, and 50 % of the nominal value of the mass flow rate. For each mass flow rate, the power was increased slowly to see its influence on MCHFR. In all cases, as power is increased, the CHFR is decreased. According to the typical thermal design limits presented by the US Nuclear Regulatory Commission (NRC) for a 100 % mass flow rate and 100 % nominal operating power, the MCHFR is within thermal-hydraulic limit [44]. While for 100 % mass flow rate it is found that the 110 % and 115 % operating power are allowable power for fuel temperature but MCHFR is less than 1.9. However, for a 75 % mass flow rate with 80 % and 85 % nominal power respectively the MCHFR is with the limit, then the MCHFR is started to be lower than the thermal-hydraulic limit. In the case of 50 % mass flow rate with all testing power levels the MCHFR is bigger than the limit. As a result, under the proposed

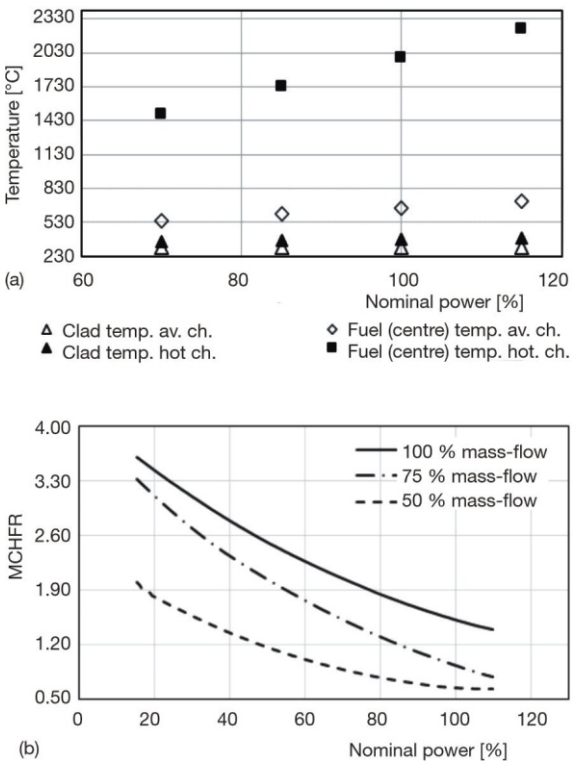

Figure 10. (a) Influence of power level on fuel (centerline and surface) and clad surface temperature in the average and hot channel, (b) Influence of power level and mass flow rate on MCHFR value. (Calculations were done under steady state operation – bottom peaked power distribution)

operating power (3579 MW), the nominal mass flow rate is sufficient to provide adequate cooling for the tested reactor *core*. while for 75 % and 50 % of nominal mass flow rate the operating power must be decreased and extreme care is needed to ensure the proper cooling is existing.

INFLUENCE OF POWER AND MASS FLOW ON PRESSURE DROP

To understand the dependency of the pressure drop across the hot and average channels on the power level and mass-flow rate the calculations were done under the different values of operating power and different value of mass flow rate for study state conditions. The obtained result is presented in tab. 5 and represented graphically in fig. 11. As coolant is forced upwardly through a fuel bundle, there is a pressure drop. A portion of this pressure drop occurs at the bottom non-boiling portion of the reactor is the single-phase pressure drop. The remaining portion of the pressure drop that occurs in the upper boiling portion of the fuel bundle is a two-phase pressure drop portion. The two-phase flow pressure drop is higher than that of single-phase flow and more complicated to calculate it.

In the boiling water reactors, the pressure drop is an important parameter for reactor safety, where both thermal-hydraulic instability and coupled nuclear-thermal-hydraulic instability are sensitive to the ratio of the single-phase pressure drop to the two-phase pressure drop in the fuel bundle.

Table 5. Influence of power and mass flow on pressure drops (bottom peaked)

Power [%]	Coolant		
	100 [%]	75 [%]	50 [%]
	P [Psi]	*P*[Psi]	*P*[Psi]
115	8.4224	7.1599	6.4505
100	8.1221	6.875	6.0459
85	7.6667	6.7175	5.4822
70	7.3274	6.5	5.2776

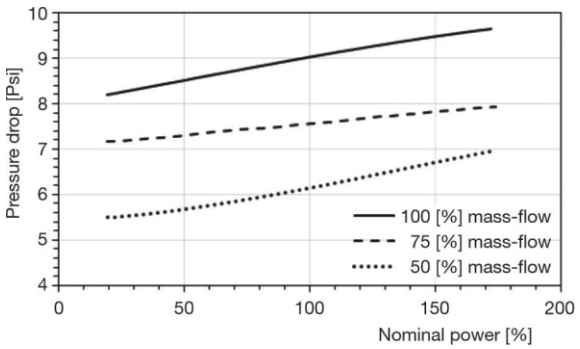

Figure 11. Influence of power level and mass flow rate on core pressure drop. (Calculations were done under steady-state operation – bottom peaked power distribution)

In the literature, it is mentioned that the thermal-hydraulic instability and coupled nuclear thermal hydraulic instabilities can be reduced by decreasing the two-phase flow pressure drop relative to the single-phase flow pressure drop [46].

Figure 11 graphically shows the influence of both power and mass-flow rate on the pressure drop. One can notice that as the operating power is increased and mass flow was kept constant, the pressure drop is increased. For the same operating power, the pressure drop decreases with decreases in mass-flow. By increasing the power and keeping the mass-flow rate constant, the length of the boiling region in the channel is increased means that the non-boiling region in the channel will be decreased. Thus, we have long distance (length) with two phases therefore the two-phase pressure drop will increase. It means that as the power is increased the ratio of the two-phase flow pressure drop to the one-phase flow pressure drop is increased. Regarding the mass-flow, when the operating power is kept constant, the pressure drop decreases as the mass-flow decreases.

CONCLUSIONS

The results obtained for the tested model BWR/6 reactor using the MITH one-dimensional thermal-hydraulic computer code show that there is very good agreement between the computer code and the data of the existing BWR/6 core's general design description.

The average and hot channel axial heat flux distributions are shown. There are some thermal-hydraulic limits presented. The applied power shape dictated the axial flux distribution. The radial peaking factor was used as input data for the hottest channel in the core. The CHFR is calculated along the channel using two CHF correlations. When all other parameters are held constant, the value of MCHFR and its position along the channel are determined by the power distribution. To determine the onset MCHFR value and position, the proper correlation is required. Because of the high vapor quality in BWR, the GE correlation result is more reliable than the W-3 result.

It's found that the 110 % and 115 % operating power are allowable power for fuel temperature and not allowable for MCHFR limit 1.9. It's found that the 75 % mass flow rate the maximum operating power should exceed 80 % and 90 % of nominal operating power to have MCHFR within the limit 1.9. In the case of 50 % mass flow rate with all testing power levels the MCHFR is over the limit. Hence, it is shown that the MCHFR is the governing factor in determining the maximum operating power and minimum mass flow rate. The pressure drop depends mainly on the operating power and mass flow rate. As a result of this study, it is concluded that the computer code MITH is reliable and can be applied, with fairly a good degree of confidence, to evaluate the thermal-hydraulic performance of existing BWR cores.

The good agreement between the obtained result and the data of the referenced reactor demonstrates the code's validity and efficiency (BWR-GE). The comparison of the code results and the data from the referenced reactor revealed good agreement with minor discrepancies, which could be explained by differences in the relevant physical parameters used in each method of calculation. In addition, we can ensure that all safety-related thermal-hydraulic parameters are within the thermal design limits for steady-state operating conditions. As a consequence, the BWR (GE) reactor is safe to operate under the previously mentioned tested operating conditions and remains within the thermal design limits.

ACKNOWLEDGMENT

The first author would like to express his heartfelt appreciation and gratitude to Eng. Mohamed Banour (M.Sc.) and Eng. Khamis Al-Thuibi (M.Sc.) at Tajoura Center for Nuclear Research – Tripoli, Libya, for their invaluable assistance. His appreciation also goes to Dr. Zoltan Hozer, head of the nuclear fuel department at Hungary's Center for Energy Research (CER) Budapest, for his insightful comments. Tony Takacs' English improvements are gratefully acknowledged by the first author. The first author would also like to thank Tajoura Nuclear Research Centre (Tripoli, Libya) for providing the code and allowing him to use their computer system network.

AUTHORS' CONTRIBUTIONS

The first author performed and made all calculations and analyses, while the second author provided the idea, supervised, and controlled the project work content. The first author wrote, reviewed, and supervised the manuscript. The first author is in responsible of the manuscript's content.

REFERENCES

[1] Moorthi, A., *et al*., A Review of Sub-Channel Thermal-Hydraulic Codes for Nuclear Reactor Core and Future Directions, *Nuclear Engineering and Design, 332* (2018), pp. 329-344, https://doi.org/10.1016/j.nucengdes.2018.03.012

[2] Khan, E. U., *et al*., LMFBR and LWR in-Core Thermal-Hydraulic Codes: The State-of-the-Art and Research and Development Needs, *Proceedings*, 20th National Heat Transfer Conference, Milwaukee, Wi., USA, 1981, https://www.osti.gov/servlets/purl/ 6170547

[3] Sha, W. T., An Overview of Rod-Bundle Thermal-Hydraulic Analysis, *Nuclear Engineering and Design, 62* (1980), 1-3, pp. 1-24

[4] Groeneveld, D. C., *et al*., AECL-UO Critical Heat Flux Look-Up Table, *Heat Transfer Engineering, 7* (1986), 1-2, pp. 46-62, DOI: 10.1080/01457638608939644

[5] McAdams, W. H., *et al*., Heat Transfer at High Rates to Water with Surface Boiling, *Industrial and Engineering Chemistry, 41* (1949), 9, pp. 1945-1953

[6] Jens, W. H., Lottes, P. A., Analysis of Heat Transfer Burnout, Pressure Drop and Density Data for High-Pressure Water, *USA EC Report ANL-4627,* (1951), pp. 1-71, https://www.osti.gov/servlets/purl/4421630

[7] Groeneveld, D. C., *et al*., An Overview of Measurements, Data Compilations and Prediction Methods for the Critical Heat Flux in Water-Cooled Tubes, *Nuclear Engineering and Design, 331* (2018), pp. 211-221, https:doi.org/10.1016/j.nucengdes.2018.02.031

[8] Guan, H. Y., Thermal Hydraulic Considerations of Nuclear Reactor Systems: Past, Present and Future Challenges, *Experimental and Computational Multiphase Flow, 1* (2019), 1, pp. 3-27, https://doi.org/10.1016/j.nucengdes.2018.03.012

[9] Nijsing, R., Temperature and Heat Flux Distribution in Nuclear Fuel Element Rods: A Calculation of Effects Due to Non-Uniform Distribution of Heat Generation, Heat Transfer Coefficient and Fuel-Cladding Contact Resistance, *Nuclear Engineering and Design, 4* (1966), 1, pp. 1-20

[10] Yadigaroglu, G. *et al*., Trends and Needs in Experimentation and Numerical Simulation For LWR Safety, *Nuclear Engineering Design, 221* (2003), 1-3, pp. 205-223

[11] Chelemer, H., *et al*., Sub-Channel Thermal Analysis of Rod Bundle Cores, *Nuclear Engineering Design, 21* (1972), 1, pp. 35-45

[12] Cheng, X., Muller, U., Review on Critical Heat Flux in Water-Cooled Reactors, FZKA- 6825, Forschngszentrum Karlsruhe GmbH, *Karlsruhe,* (2003), pp. 1-33, http://digbib.ubka.uni-karlsruhe.de/volltexte/fzk/6825/6825.pdf

[13] Helmy, S., *et al*., Analysis of Thermal Hydraulic Behavior of KONVOI PWR During a Design Extension Condition, *Nucl Technol Radiat, 36* (2021), 1, pp. 1-11

[14] Hutli, E., Kridan, R., Thermal-Hydraulic Analysis of Light Water Reactors Under Different Steady-State Operating Condition, Part 2 – Pressurized Water Reactor, *Nucl Technol Radiat*, *37* (2022), 4, pp. 276-288

[15] Seung, H. A., Gyoo-Dong, J., Effect of Spacer Grids on CHF at PWR Operating Conditions, *Nuclear Engineering and Technology, 33* (2001), 3, pp. 283-297

[16] Weisman, J., Ying, S. H., A Theoretically Based Critical Heat Flux Prediction for Rod Bundles at PWR Conditions, *Nuclear Engineering Design, 85* (1984), 2, pp. 239-250

[17] Hejzlar, P., Todreas, N. E., Consideration of Critical Heat Flux Margin Prediction by Subcooled or Low-Quality Critical Heat Flux Correlations, *Nuclear Engineering Design, 163* (1996), 1-2, pp. 215-223

[18] Khabensky, V. B., *et al*., Critical Heat Flux Prediction in Vertical Bottom-Closed Rod Bundles, *Nuclear Engineering Design, 182* (1998), 3, pp. 203-224

[19] Chaudri, K. S., *et al*., Development of Sub-Channel Code Sacos and Its Application in Coupled Neutronics / Thermal-Hydraulics System for SCWR, *Annals of Nuclear Energy, 45* (2012), pp. 37-45, https://doi.org/10.1016/j.anucene.2012.02.014

[20] Kim, H. C., *et al*., Critical Heat Flux Water in Vertical Round Tubes at Low Pressure and Low Flow Conditions, *Nuclear Engineering Design, 199* (2000), 1-2, pp. 49-73

[21] Ezsol, G., *et al*., Measurements for Verification and Validation of Thermal-Hydraulic Computer Code Used for Thermal-Hydraulic Analysis of VVER440

Typical Fuel Assembly, *Measurement, 171* (2021), pp. 1-14, https://doi.org/10.1016/j.measurement.2020.108787
[22] Tseng, Y. S., *et al*., Investigating Flow and Heat Transfer Characteristics in a Fuel Bundle with Split-Vane Pair Grids by CFD Methodology, *Annals of Nuclear Energy, 64* (2014), pp. 93-99, https://doi.org/10.1016/j.anucene.2013.09.037
[23] Roidt, M., *et al*., Determination of Turbulent Exchange Coefficients in a Rod Bundle, *Journal of Heat Transfer ASME. 96* (1974), 2, pp. 172-177
[24] Hutli, E., *et al*., Experimental Approach to Investigate the Dynamics of Mixing Coolant Flow in Complex Geometry Using PIV and PLIF Techniques, *Thermal Science International Scientific Journal, 19* (2014), 3, pp. 989-1004, https://doi.org/10.2298/TSCI130603051H
[25] Roidt, R. M., *et al*., Experimental Investigations of the Hydraulic Field in Wire-Wrapped LMFBR Core Assemblies, *Nuclear Engineering Design, 62* (1980), 1-3, pp. 295-321
[26] Conner, M. E., *et al*., CFD Methodology and Validation for Single-Phase Flow in PWR Fuel Assemblies, *Nuclear Engineering Design, 240* (2010), 9, pp. 2088-2095
[27] Ikeda, K., *et al*., Single-Phase CFD Applicability for Estimating Fluid Hot-Spot Locations in a 5 × 5 Fuel Rod Bundle, *Nuclear Engineering Design, 236* (2006), 11, pp. 1149-1154
[28] Toth, S., Aszodi, A., CFD Analysis of Flow Field in A Triangular Rod Bundle, *Nuclear Engineering Design, 240* (2010), 2, pp. 352-363
[29] Hutli, E., *et al*., Experimental and Numerical Investigation of Coolant Mixing in a Model of Reactor Pressure Vessel Down-Comer and in Cold Leg Inlets, *Thermal Science Scientific Journal, 21* (2017), 3, pp. 1491-1502
[30] Farkas, I., *et al*., The Applicability of CFD to Simulate and Study the Mixing Process and the Thermo-Hydraulic Consequences of a Main Steam Line Break in PWR Model, *Thermal Science International Scientific Journal, 21* (2017), 6-B, pp. 3025-3036
[31] Farkas, I., Validation of Computational Fluid Dynamics Calculation Using Rossendorf Coolant Mixing Model Flow Measurements in Primary Loop of Coolant in a Pressurized Water Reactor Model, *Nuclear Engineering and Technology, 48* (2016), 4, pp. 941-951
[32] Duderstadt, J. J., Hamilton, L. J., *Nuclear Reactor Analysis*, John Wiley & Sons, Inc, USA 1976, Appendix H, pp. 634-635
[33] Tentner, A., *et al*., Advances in Computational Fluid Dynamics Modeling of Two-Phase Flow in a Boiling Water Reactor Fuel Assembly, *Proceedings of ICONE14*, International Conference on Nuclear Engineering, Miami, Fla., USA, 2006, ICONE14-89158
[34] Hiroyuki, Y., *et al*., Numerical Evaluation of Fluid Mixing Phenomena in Boiling Water Reactor Using Advanced Interface Tracking Method, *Journal of Fluid Science and Technology, 3* (2008), 2, pp. 311-322
[35] Mitsuyasu, T., *et al*., A Coupling Model for the Two-Stage Core Calculation Method with Sub-channel Analysis for Boiling Water Reactors, *Annals of Nuclear Energy, 102* (2017), pp. 77-84
[36] Bozzola S., Fundamentals of Boiling Water Reactor (BWR), International Atomic Energy Agency (IAEA), 1982, https://inis.iaea.org/search/search.aspx?orig_q=RN:15025513 https://inis.iaea.org/collection/NCLCollectionStore/_Public/15/025/15025513.pdf?r=1&r=1
[37] Belblidia, L. A., Bratianu, C., Density-Wave Oscillations, *Annals of Nuclear Energy, 6* (1979), 7-8, pp. 425-444 https://reader.elsevier.com/reader/sd/pii/0306454979900392?token=0DA3CF7E59A47F485464AADD60DF815A267C295FA1893B3E4E8FE0CB64ED70417893AE6AE33BE7087883097BA76A1AE6
[38] Winterton, R. H. S., Thermal Design of Nuclear Reactors, Reactor Systems, Elsevier Ltd. USA, 1981, pp. 11-23 https://doi.org/10.1016/B978-0-08-024215-6.50006-1
[39] ***, Technical Training Center, United States Nuclear Regulatory Commission, BWR/4 Technology Manual (R-104b), 2010 https://www.nrc.gov/docs/ML0228/ML022830867.pdf
[40] ***, ATI Inc. (Allegheny Technologies Incorporated), Zirconium Alloys, Reactor Grade Zirconium, Technical Data Sheet, Version 1, 2015, pp. 1-3 https://www.atimaterials.com/Products/Documents/datasheets/zirconium/alloy/Zr_nuke_waste_disposal_v2.pdf
[41] ***, U.S. Department of Energy Office of Environmental Management, Depleted Uranium Hexafluoride Management Program, Characteristics of Uranium and Its Compounds, Depleted Uranium Hexafluoride Fact Sheet, 2001, pp.1-4 https://web.evs.anl.gov/uranium/pdf/UraniumCharacteristicsFS.PDF
[42] ***, Nuclear Energy Agency (NEA), Nuclear Fuel Safety Criteria Technical Review, *Nuclear Safety, Second Edition,* (2012), ISBN 978-92-64-99178-1 Nuclear Fuel Safety Criteria.pdf
[43] Tong L. S., Weisman, J., Thermal Analysis of Pressurized Water Reactors, 3rd Edition, American Nuclear Society, 555 North Kensington Avenue, La Grange Park, Illinois 60525 USA, 1996
[44] Todreas, N. E., Kazimi, M. S., Nuclear Systems I – Thermal Hydraulics Fundaments, Taylor&Francis, 2nd Printing, (USA), 1993, pp.19-71
[45] Kok, K. D., Heat Transfer and Thermal Hydraulic Analysis, Nuclear Engineering Handbook, Chapter 20, CRC Press Taylor & Francis Group, 2009, pp. 642-709
[46] Dix, G. E., *et al*., Two-Phase Pressure Drop Reduction BWR Assembly Design, General Electric Company, European Patent Application, 1992 https://patentimages.storage.googleapis.com/c0/30/48/f715e1a6f8f346/EP0336203A2.pdf

Received on June 17, 2022
Accepted on November 28, 2022

Ездин ХУТЛИ, Рамадан КРИДАН

ТЕРМАЛНОХИДРАУЛИЧНА АНАЛИЗА ЛАКОВОДНОГ РЕАКТОРА У СТАБИЛНИМ РАДНИМ УСЛОВИМА
Први део – реактор са кључалом водом

У раду је приказана термохидраулична анализа стационарног стања BWR/6 језгра реактора са кључалом водом при номиналним радним условима. BWR/6 реактор производи Џенерал Електрик – САД. Циљ анализе је да се маргина термичке сигурности одржи под контролом и интегритет језгра нетакнут у условима стабилног рада. Испитани су утицаји радних услова: расподела снаге, ниво снаге и проток масе расхладне течности на перформансе предложеног језгра. У ту сврху коришћен је MITH једнодимензионални компјутерски код. Поузданост кода проверена је коришћењем бенчмарка – Џенерал Електрик реактора од 3579 MW. Тестирани су двоканални модели, просечан и врућ канал. Термохидраулични параметри, као што су средишња линија горива, површина горива, спољашња површина омотача, температура хладиоца, критични и стварни локални топлотни ток, одступање и критичан и минимално критичан однос топлотног флукса и пад притиска, процењени су дуж тестираних канала. Одређене су температуре, као и стварни и критични профили расподеле топлотног флукса. Радни услови који су испитивани имали су значајан утицај на ове параметре, такође и на термохидрауличне перформансе. Добијени резултати су у доброј сагласности са подацима тестираног језгра и налазе се ваљано у границама сигурности. Добро слагање између података о тестираном реактору и прорачуна MITH кода који се тичу реактора, показује поузданост методологије анализе из термохидрауличне перспективе.

Кључне речи: гориво, кошуљица, хладилац, снага, топлотни флукс, минимално критичан однос топлотног флукса